This paper is published as part of a *CrystEngComm* themed issue on:

Crystal Engineering in Molecular Magnetism

Guest Editors Concepció Rovira and Jaume Veciana
Institut de Ciència de Materials de Barcelona (ICMAB), Spain

Published in issue 10, 2009 of *CrystEngComm*

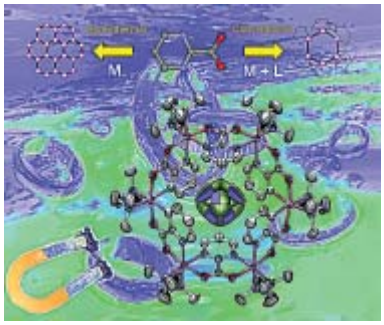

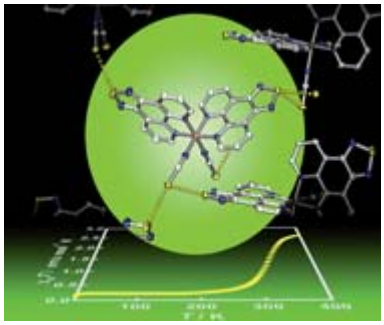

Images reproduced with permission of Enrique Colacio (left) and Kunio Awaga (right)

Papers published in this issue include:

Towards high T_c octacyanometalate-based networks
Barbara Sieklucka, Robert Podgajny, Dawid Pinkowicz, Beata Nowicka, Tomasz Korzeniak, Maria Bałanda, Tadeusz Wasiutyński, Robert Pełka, Magdalena Makarewicz, Mariusz Czapla, Michał Rams, Bartłomiej Gaweł and Wiesław Łasocha, *CrystEngComm*, 2009, DOI: 10.1039/b905912a

Cooperativity from electrostatic interactions: understanding bistability in molecular crystals
Gabriele D'Avino, Luca Grisanti, Anna Painelli, Judith Guasch, Imma Ratera and Jaume Veciana, *CrystEngComm*, 2009, DOI: 10.1039/b907184a

Anion encapsulation promoted by anion···π interactions in rationally designed hexanuclear antiferromagnetic wheels: synthesis, structure and magnetic properties
Enrique Colacio, Hakima Aouryaghal, Antonio J. Mota, Joan Cano, Reijo Sillanpää and A. Rodríguez-Diéguez, *CrystEngComm*, 2009, DOI: 10.1039/b906382j

Fe(II) spincrossover complex of [1,2,5]thiadiazolo[3,4-*f*][1,10]phenanthroline
Yoshiaki Shuku, Rie Suizu, Kunio Awaga and Osamu Sato, *CrystEngComm*, 2009, DOI: 10.1039/b906845g

Visit the *CrystEngComm* website for more cutting-edge crystal engineering research
www.rsc.org/crystengcomm

A new hybrid molecular metal assembling a BEDT-TTF conducting network and the magnetic chain anion $[Mn_2Cl_5(H_2O)_5]^-_\infty$: α-(BEDT-TTF)$_2$[$Mn_2Cl_5(H_2O)_5$]†

Leokadiya V. Zorina,*[a] Tat'yana G. Prokhorova,[b] Salavat S. Khasanov,[a] Sergey V. Simonov,[a] Vladimir N. Zverev,[a] Alexey V. Korobenko,[ac] Anna V. Putrya,[ac] Vladimir S. Mironov,[d] Enric Canadell,[e] Rimma P. Shibaeva*[a] and Eduard B. Yagubskii[b]

Received 24th March 2009, Accepted 3rd June 2009
First published as an Advance Article on the web 3rd July 2009
DOI: 10.1039/b905840k

The synthesis, X-ray crystal and electronic band structures as well as magnetotransport and magnetic properties of the α-(BEDT-TTF)$_2$[$Mn_2Cl_5(H_2O)_5$] radical cation salt with a new type of magnetic polymeric complex anion, $[Mn_2Cl_5(H_2O)_5]^-_\infty$, are reported. The crystal structure is characterized by radical cation layers alternating with layers of the polymeric 1-D chain anions constructed from $MnCl_3(H_2O)_3$ and $MnCl_4(H_2O)_2$ octahedra connected to each other *via* the apical Cl atoms. The calculated electronic band structure suggests that the salt should be a stable 2-D metal and the conductivity measurements show that it exhibits metallic behavior down to 0.4 K. Shubnikov-de Haas oscillations, observed at $B > 10$ T, are characterized by two fundamental frequencies, corresponding to cross-sections of the Fermi surface, in agreement with the electronic band structure calculations. Magnetic measurements reveal antiferromagnetic correlations in the anion network.

Introduction

A large interest is currently devoted to hybrid multifunctional materials combining different physical properties. The family of low-dimensional radical cation salts based on organic π-donors with paramagnetic metal complex anions is an important class of such materials.[1] Since in these molecular systems the spins of the conducting network are polarized by the magnetic layers, these compounds are regarded as promising candidates for molecular electronics (spintronics). In recent years a steady progress in the study of organic magnetic conductors has been achieved. Several organic charge-transfer salts with anions containing magnetic ions have been synthesized and characterized. Significant new results have been obtained by using the magnetic anions $[MX_4]^{n-}$ (X = Cl, Br; M: transition metal), $[MX(CN)_5]^{3-}$ (X = CN, NO), $[M(C_2O_4)_3]^{3-}$, and $[M^{II}M^{III}(C_2O_4)_3]^{3-}$ as well as polyoxometalates. For instance, the following paramagnetic metals have been obtained: (BEDT-TTF)$_3$$CuCl_4\cdot H_2O$,[2] (BDH-TTP)$_2$$FeCl_4$,[3] (BET-TTF)$_2$$FeCl_4$,[4] β″-(BEDO-TTF)$_{2.42}${$K_2$[$CrNO(CN)_5$]},[5] β″-(BEDO-TTF)$_6$$(H_3O^+)_x[M(CN)_6]\cdot G_{2-x}$ (G is a guest solvent molecule),[6] (BEDO-TTF)$_3$$[Fe^{II}Cr^{III}(C_2O_4)_3](H_2O)_{3.5}$[7] and β″-(BEDT-TTF)$_5$$[H_3V_{10}O_{28}]\cdot 4H_2O$.[8] It has also been demonstrated that superconductivity and paramagnetism coexist in the isostructural radical cation salts β″-(BEDT-TTF)$_4$$H_3O^+[M(C_2O_4)_3]\cdot G$, (M = Fe, Cr).[1b,9] The antiferromagnetic superconductors κ-(BETS)$_2$$FeX_4$ (X = Cl, Br),[1d,10] κ-(BETS)$_2$$Mn[N(CN)_2]_3$[11] and β-(BDA-TTP)$_2$$FeCl_4$[12] have been synthesized, and magnetic field induced superconductivity has been recently found in λ-(BETS)$_2$$FeCl_4$[1d,13] and κ-(BETS)$_2$$FeBr_4$.[10] In addition, the first layered ferromagnetic organic metals with bimetallic oxalates, $(D)_x[M^{II}Cr(C_2O_4)_3]\cdot G$ (D = BEDT-TTF and BETS; $x \approx 3$), have been discovered.[14]

As a part of our general research effort intending to extend the range of molecular materials combining two properties in the same crystal, we have recently obtained the α-(BEDT-TTF)$_2$[$Mn_2Cl_5(H_2O)_5$] (**1**) radical cation salt. Although there are a number of BEDT-TTF-based conducting charge transfer salts with magnetic chloromanganate(II) anions,[15] the title compound is an interesting example because it includes a new type of magnetic polymeric complex $[Mn_2Cl_5(H_2O)_5]^-_\infty$ as counterion and exhibits stable metallic properties down to 0.4 K. Herein, we report the synthesis, crystal and electronic structures, magnetotransport and magnetic properties of this new hybrid molecular system.

Experimental

Synthesis

Starting compounds, BEDT-TTF, $MnCl_2\cdot 4H_2O$, $(NH_4)_3[Fe(ox)_3]\cdot 3H_2O$, $FeCl_3\cdot 6H_2O$, NH_4Cl, chlorobenzene (CB), benzonitrile (BN) and 1,2,4-trichlorobenzene (TCB) were used as received (Aldrich); 18-crown-6 (Aldrich) was purified by recrystallization from acetonitrile and dried in vacuum at 30 °C over P_2O_5.

Crystals of the radical cation salt **1** were grown following the method of electro-crystallization in conventional H-shaped cells

[a]*Institute of Solid State Physics, RAS, Chernogolovka, MD, 142432, Russia. E-mail: zorina@issp.ac.ru; shibaeva@issp.ac.ru*
[b]*Institute of Problems of Chemical Physics, RAS, Chernogolovka, MD, 142432, Russia*
[c]*Moscow Institute of Physics and Technology, Dolgoprudny, Moscow Region, Russia*
[d]*Institute of Crystallography, RAS, Leninsky pr., 59, Moscow, 119333, Russia*
[e]*Institut de Ciència de Materials de Barcelona, CSIC, Campus de la UAB, E-08193 Bellaterra, Spain*

† CCDC reference number 723863. For crystallographic data in CIF or other electronic format see DOI: 10.1039/b905840k

with Pt electrodes. The electro-oxidation of BEDT-TTF (2.5×10^{-5} M) was carried out at a constant current (0.3–0.5 μA) and at fixed temperature (~25 ° C) in the presence of different supporting electrolytes. The following three kinds of electrolytes were examined: (1) $(NH_4)_3[Fe(ox)_3]\cdot 3H_2O$ (2.3×10^{-4} M) + $MnCl_2\cdot 4H_2O$ (2.5×10^{-4} M) + 18-crown-6 (6.9×10^{-4} M) in the mixture of solvents: BN, TCB and EtOH in a 1 : 2 : 0.3 molar ratio (33 ml); (2) $FeCl_3\cdot 6H_2O$ (1.8×10^{-4} M) + $MnCl_2\cdot 4H_2O$ (2.5×10^{-4} M) + 18-crown-6 (5.6×10^{-4} M) + NH_4Cl (5.4×10^{-4} M) in CB (25 ml) + 10 v/v % EtOH; (3) $MnCl_2\cdot 4H_2O$ (2.5×10^{-4} M), NH_4Cl (5×10^{-4} M) and 18-crown-6 (5×10^{-4} M) in the mixture of solvents: TCB, CB and EtOH (1 : 1 : 0.2, 22 ml). The third case is the most convenient one. Good quality single crystals were obtained at a constant current of 0.5 μA after 2 weeks. The use of the electrolytes (1) and (2) was associated with attempts to prepare the BEDT-TTF salts containing bimetallic oxalato (or chloro) complexes as counter ions. However, crystals of α-(BEDT-TTF)$_2$[$Mn_2Cl_5(H_2O)_5$] were formed in these cases.

X-Ray crystallography and band structure calculations

Crystal data of 1. $C_{20}H_{26}Cl_5Mn_2O_5S_{16}$, $M = 1146.50$, orthorhombic, $Cmc2_1$, $a = 78.612(3)$, $b = 10.6365(5)$, $c = 9.6012(4)$ Å, $V = 8028.1(6)$ Å^3, $Z = 8$, $D_{calc} = 1.897$ g cm^{-3}, $\mu = 18.29$ cm^{-1}, $F(000) = 4616$, $T = 295(2)$ K, $2\theta_{max} = 58.74°$, reflections measured 43 900, unique reflections 9507 ($R_{int} = 0.0446$), reflections with $I > 2\sigma(I) = 7186$, parameters refined 520, $R_1 = 0.0504$, $wR_2 = 0.1336$, GOF = 1.052, Flack x parameter 0.41(3).

X-Ray experimental data were collected on a single crystal ($0.8 \times 0.4 \times 0.4$ mm^3) at room temperature using an Oxford Diffraction Gemini-R diffractometer equipped with a Ruby CCD detector [λ(Mo Kα) = 0.71073 Å, graphite monochromator, ω-scans]. Data reduction with empirical absorption correction of experimental intensities (Scale3AbsPack program) was made with the CrysAlisPro software.[16] The structure was solved by a direct method followed by Fourier syntheses and refined by a full-matrix least-squares method in an anisotropic approximation for all non-hydrogen atoms, with the SHELX-97 programs.[17] The positions of the H-atoms were calculated geometrically in the terminal ethylene parts of BEDT-TTF and restrained by DFIX instructions in the H_2O groups of the anion in the ordered anion layer, U_{iso}(H) were fixed at $1.2U_{eq}$(C) or $1.5U_{eq}$(O). In the disordered anion layer the water hydrogen atoms were not defined. The compound crystallizes in the non-centrosymmetric space group $Cmc2_1$ and racemic twinning is present; the enantiomorphic domain scale factor is refined to 0.41(3). Note that the diffraction pattern consists of two types of reflections: sharp and intense diffraction peaks with $k = 2n$, which describe an average structure, and lines of weak and spread additional reflections with $k = 2n + 1$ whose topology and intensity varied from synthesis to synthesis. All weak reflections, along with the strong ones, were included into the $Cmc2_1$ refinement revealing positional ordering both inside and between the anion layers. Previously, the unit cell parameters were published in the monoclinic setting: $P2_1/c$, $a = 10.637$, $b = 9.601$, $c = 39.667$ Å, $\beta = 97.73°$, $V = 4014.2$ Å^3, $Z = 4$.[18]

The tight-binding band structure calculations were based upon the effective one-electron Hamiltonian of the extended Hückel method.[19] The off-diagonal matrix elements of the Hamiltonian were calculated according to the modified Wolfsberg-Helmholz formula.[20] All valence electrons were explicitly taken into account in the calculations and the basis set consisted of double-ζ Slater-type orbitals for C and S and single-ζ Slater-type orbitals for H. The exponents, contraction coefficients and atomic parameters for C, S and H were taken from the previous work.[21]

Transport and magnetic measurements

Sample resistance was measured using a four-probe technique by a lock-in detector at 20 Hz alternating current. The resistance measurements in the temperature range (0.4–300 K) were carried out in a cryostat with a superconducting solenoid, which generated a magnetic field of up to 17.2 T.

The temperature dependence of the magnetic moment was studied using a Quantum Design MPMS 5XL SQUID magnetometer in a constant magnetic field ($H = 1$ kOe) at 2–300 K. The measurements were performed on polycrystalline samples.

Results and discussion

Crystal and electronic band structure

The structure of α-(BEDT-TTF)$_2$[$Mn_2Cl_5(H_2O)_5$] (**1**) crystals is made of radical cation layers alternating along the a-axis with layers of the polymeric chain anions $[Mn_2Cl_5(H_2O)_5]^-_\infty$ (Fig. 1). The asymmetric unit includes two independent donor molecules in general positions, the [$Mn_2Cl_5(H_2O)_5$] anion in a half-occupied general position and half of the anion unit in a special position on the m-plane. The unit cell contains four donor layers and four anion layers, one donor layer and two anion layers being symmetrically independent.

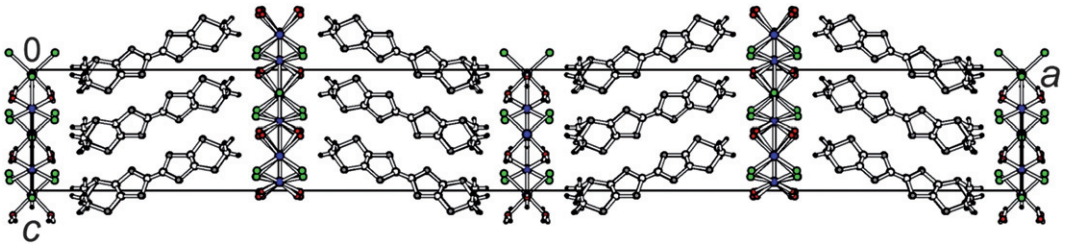

Fig. 1 The layered structure of **1** projected along the b axis.

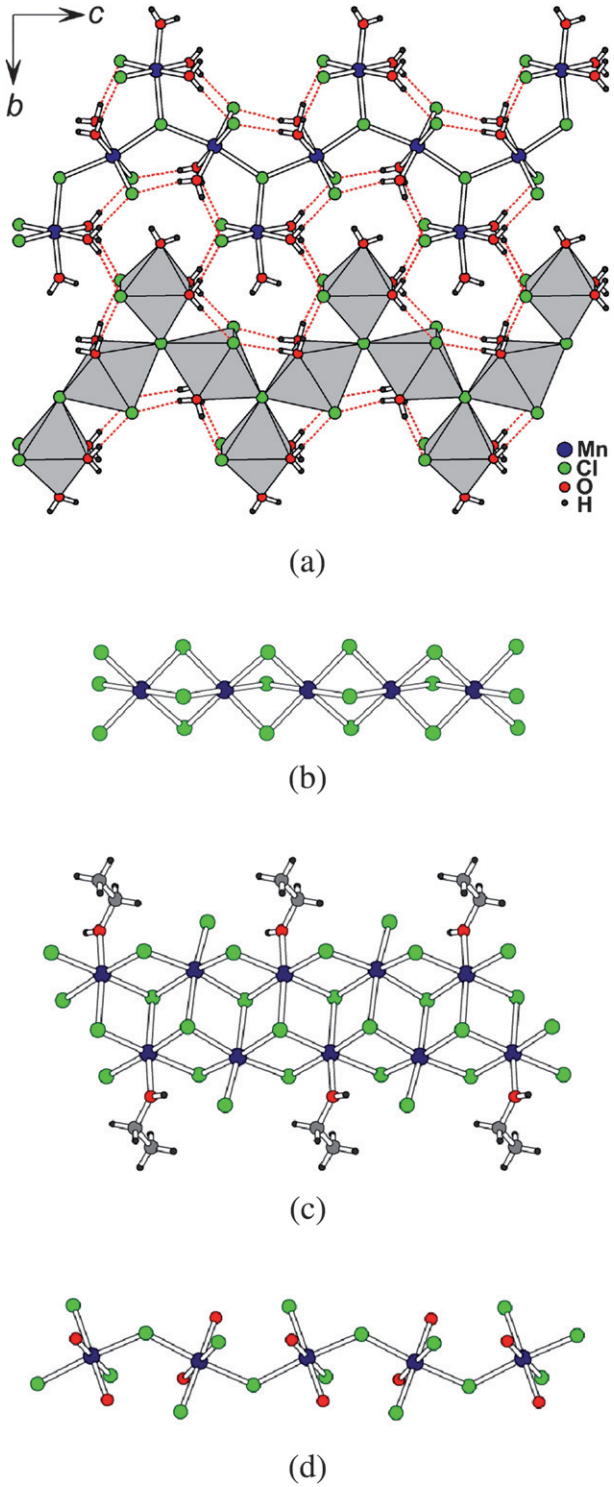

Fig. 2 (a) The anion layer $[Mn_2Cl_5(H_2O)_5]^-{}_\infty$ in **1** with two different representations (atoms and polyhedra) of the symmetry related infinite anion chains. The dotted lines highlight the O–H···Cl hydrogen bonds (see Table 1 for the hydrogen bonds geometry). (b–d) Some known types of infinite chloromanganate 1-D chains: (b) $[MnCl_3]^-{}_\infty$ chain of face-shared octahedra in $[(CH_3)_4N][MnCl_3]$[23] and δ-(BEDT-TTF)$_3$[$MnCl_3$]$_2$(C_2H_5OH);[15d] (c) $[Mn_2Cl_5(C_2H_5OH)]^-{}_\infty$ chain of edge-shared octahedra in β-(BEDT-TTF)$_2$[Mn_2Cl_5(C_2H_5OH)];[15c] (d) chain of corner-shared $[MnCl_4(H_2O)_2]$ octahedra in α-Rb[$MnCl_3$(H_2O)$_2$].[23b,24]

Both anion layers contain infinite anion chains $[Mn_2Cl_5(H_2O)_5]^-{}_\infty$ running along the *c* direction. Fig. 2a gives two different representations of the symmetry related chains in the anion layer. The zigzag chains are constructed from $MnCl_3(H_2O)_3$ and $MnCl_4(H_2O)_2$ octahedra connected to each other *via* apical Cl atoms. The independent anion layers differ by symmetry and degree of disorder. Anion layers on mirror *m*-planes ($x = 0, 0.5$) are almost completely ordered while the other two layers ($x = 0.25, 0.75$) lie on *b* glide planes and inside these layers two equivalent anion chains with half occupation are mutually displaced by a half-translation along *b*. The observed positional disorder is not induced by the high $Cmc2_1$ symmetry but really occurs in the structure since the same disorder remains upon symmetry lowering.

Within the zigzag chain the Mn atom positions form almost equilateral triangles with Mn···Mn distances of 4.604(1), 4.636(1) and 4.825(1) Å. The bridging Mn–Cl–Mn angle along the chain is 123.03(5)° while similar angles with the lateral fragments are 117.59(6) and 119.38(6)°. The interchain Mn···Mn distance is 5.553(1) Å. The Mn–Cl interatomic distances to the bridging Cl atom shared by three octahedra are 2.739(2), 2.751(2) Å in $[MnCl_4(H_2O)_2]$ and 2.631(2) Å in $[MnCl_3(H_2O)_3]$, while the Mn–Cl distances to the terminal Cl atoms are 2.463(1) and 2.491(1) Å in the former and the latter octahedra, respectively. A similar tendency to increase the Mn–Cl bond distance upon increasing the number of Mn atoms in the coordination sphere of Cl has been observed earlier in different structural motifs from $[MnCl_xO_{6-x}]$ octahedra including infinite chains of different geometry.[22]

A stable strictly regular distribution of the ligands along the chains is observed: water ligands always occur between chlorines and *vice versa*. Owing to this specific positional ordering, all octahedra within the anion layer are self-assembled and well connected by numerous hydrogen bonds from H_2O molecules to Cl atoms (dotted lines in Fig. 2a) which occur inside and between the chains. The geometrical details of these hydrogen bonds are described in Table 1. This kind of extensive hydrogen bonding is typical of infinite chains formed by corner-linked Mn octahedra with mixed chlorine–water ligands and is responsible for the folding of the chains into a zigzag configuration.

Up to now a number of BEDT-TTF-based radical cation salts with chloromanganate(II) anions have been synthesized and structurally characterized: β′-(BEDT-TTF)$_3$[$MnCl_4$]$_2$ (**2**),[15a] β″-(BEDT-TTF)$_3$[$MnCl_4$]($C_2H_3Cl_3$) (**3**),[15b] β-(BEDT-TTF)$_2$[Mn_2Cl_5-(C_2H_5OH)] (**4**),[15c] δ-(BEDT-TTF)$_3$[$MnCl_3$]$_2$(C_2H_5OH) (**5**),[15d] (BEDT-TTF)$_4$[$MnCl_4$](CH_2Cl_2)$_2$ (**6**),[15e] α′-(BEDT-TTF)$_7$[$MnCl_4$]$_2$-($C_2H_3Cl_3$)$_2$ (**7**).[15f] The crystals **2**, **3**, **5** and **6** are semiconductors,

Table 1 Geometry of hydrogen O–H···Cl bonds in the anion layer of **1**.[a,b]

O–H···Cl	H···Cl/Å	O···Cl/Å	O–H···Cl/°
O1 H1a Cl3	2.28(2)	3.093(4)	170(5)
O1 H1b Cl2^{i}	2.37(3)	3.124(3)	153(5)
O2 H2a Cl2^{ii}	2.30(2)	3.111(4)	167(5)
O2 H2b Cl3^{iii}	2.37(4)	3.132(4)	152(6)

[a] O–H bond lengths were restrained to values of 0.82(1) Å. [b] Symmetry operations: (i) x, $1 - y$, $0.5 + z$; (ii) $-x$, $-y$, $0.5 + z$; (iii) $-x$, $-y$, $z - 0.5$.

while the crystals **4** and **7** exhibit metallic properties down to 2 K (at ambient pressure) and 1.2 K (≥2.9 kbar), respectively. The anion part of crystals consists of discrete tetrahedra $[MnCl_4]^{2-}$ (in **2**, **3**, **6**, **7**) or different polymeric chains (in **4**, **5**). It should be noted that the salts **3**, **5** and **7** are unexpectedly obtained when the straightforward electrochemical synthesis started from BEDT-TTF and the "Mn_{12}"-cluster. In our case, the single crystals **1** were also initially accidentally obtained during an attempt to have the BEDT-TTF salt with bimetallic complexes of the $[M^{II}M^{III}(C_2O_4)_3]^-$ type. Luckily, the title BEDT-TTF salt has been found to include a novel magnetic polymeric anion of Mn^{II}. Some previously known types of polymeric chains in chloromanganates(II) are shown in Fig. 2b–d. The structural features of the infinite chain from $[MnCl_6]$ octahedra in **5** (Mn···Mn 3.359 Å) are quite similar to those of linear chain antiferromagnets such as $[(CH_3)_4N][MnCl_3]$[23] (Fig. 2b). The antiferromagnetic 1-D chain in **4**[15c] is described as $[Mn_2Cl_5(C_2H_5OH)]^-_\infty$ and composed of $[MnCl_6]$ and $[MnCl_5(C_2H_5OH)]$ octahedra (Fig. 2c) (Mn···Mn 3.716, 3.800, 3.744, 3.907 and 3.960 Å). The Mn···Mn distance in the 1-D chain of α-Rb$[MnCl_3(H_2O)_2]$[24] is 4.538 Å (Fig. 2d).

The organic BEDT-TTF layer of crystal **1** has an α-type packing and is composed of inclined donor stacks (Fig. 3). Two independent BEDT-TTF radical cations are nearly flat (the folding around the S–S lines between the central and outer parts of the BEDT-TTF fragments is close to 3°) and have the same charge, 0.5^+, according to the stoichiometry of the compound and analysis of the bond lengths in the TTF-cores following the formula proposed by Guionneau *et al.*[25] From the symmetry point of view the stack is not uniform but symmetrically non-equivalent intrastack interactions show the same characteristics: large and almost equal interplane separations of 3.81(4) and 3.85(4) Å and similar overlapping mode with only transversal molecular displacement, which is very strong since the interplanar angle between molecules from adjacent stacks is very large for α-phases (88°). There are many short S···S intermolecular contacts (≤3.70 Å) between the stacks in the radical cation layer, which are shown as dotted lines in Fig. 3, and listed in Table 2

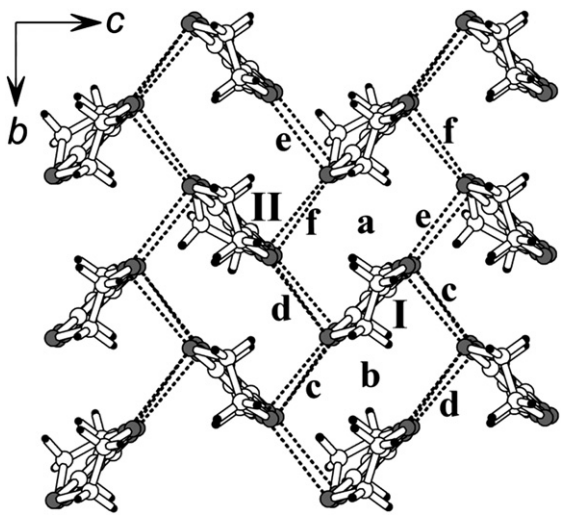

Fig. 3 The radical cation layer of **1**. Short S···S interstack contacts are shown by dotted lines. Non-equivalent intermolecular interactions are labeled from a to f (see Table 2 for the interaction energies).

Table 2 Intermolecular S···S contacts shorter than 3.70 Å and absolute values of the transfer integrals $|\beta_{HOMO-HOMO}|$ for the different donor··· donor interactions a–f (see Fig. 3) in the radical cation layer of **1**

Interaction	S···S contact distances/Å	$\lvert\beta_{HOMO-HOMO}\rvert$/eV
a	—	0.1653
b	—	0.1566
c	3.549(2), 3.634 (3), 3.659(2)	0.2265
d	3.561(2), 3.648(3), 3.696(2)	0.2270
e	3.534(2), 3.663(2)	0.2240
f	3.556(2), 3.667(3)	0.2198

while the shortest intrastack S···S distance is 3.870(2) Å. The long molecular axes of BEDT-TTF from adjacent layers are not parallel (Fig. 1) and the associated angle is 44°. The donor and anion layers interact through hydrogen contacts from ethylene groups of BEDT-TTF radical cations to anion ligands; the shortest (C)H···O and (C)H···Cl distances correspond to 2.72 and 2.85 Å, respectively.

Note that few radical cation salts with conducting layers of α type have been structurally characterized. Thus, the comparison of the present α-phase with the well known isostructural family of molecular metals α-(BEDT-TTF)$_4$[MHg(SCN)$_4$] (M = NH_4^+, K^+, Rb^+ and Tl^+), which exhibit many intriguing physical properties[1a] (Shubnikov-de-Haas effect, gigantic angle-dependent magnetoresistance oscillations, magnetic phase transitions,[26] magnetic field-induced CDW transitions and superconductivity[27]), is worthwhile doing.

The calculated band structure for a donor layer of **1** is shown in Fig. 4a. This band structure shows both similarities and differences with those for other α-phases calculated with the same computational approach.[28] An important difference concerns the bandwidth along the two main axes of the BEDT-TTF sublattice (*i.e.* b^* ($\Gamma \rightarrow Y$) and c^* ($\Gamma \rightarrow Z$)), which is now more typical of a two-dimensional system. This is mainly due to the fact that in **1** there are no band gaps at the ***Y*** or ***Z*** points. This makes the situation somewhat different from that in classical α-phases, such as α-(BEDT-TTF)$_2$[KHg(SCN)$_4$]. In order to more closely analyze the relationship between the crystal and band structure we have evaluated the strength of the six different HOMO···HOMO intermolecular interactions in the donor layers. The absolute values of the $\beta_{HOMO-HOMO}$ interaction energies[29] as well as the S···S contacts shorter than 3.7 Å are reported in Table 2. These results clearly show that the four types of the interstack interactions (c–f) are very close in magnitude. In addition, interactions a and b within the stacks are much more uniform and are considerably stronger than in the related α-phases. The highly isotropic two-dimensional network of HOMO–HOMO interactions in the present salt is a quite unique situation among α-type salts. It is interesting to note that, albeit being associated with long S···S contacts (*ca* 3.9 Å), the intrastack interactions are quite strong. This is due to the occurrence of four strong S···S contacts, all of which have an almost pure σ-character. These contacts are the result of lateral displacements of the BEDT-TTF molecules, which occur in such a way that the sulfur atoms of the upper molecule are almost straight above the sulfur atoms of the lower molecule. This provides strong interactions within the stacks.

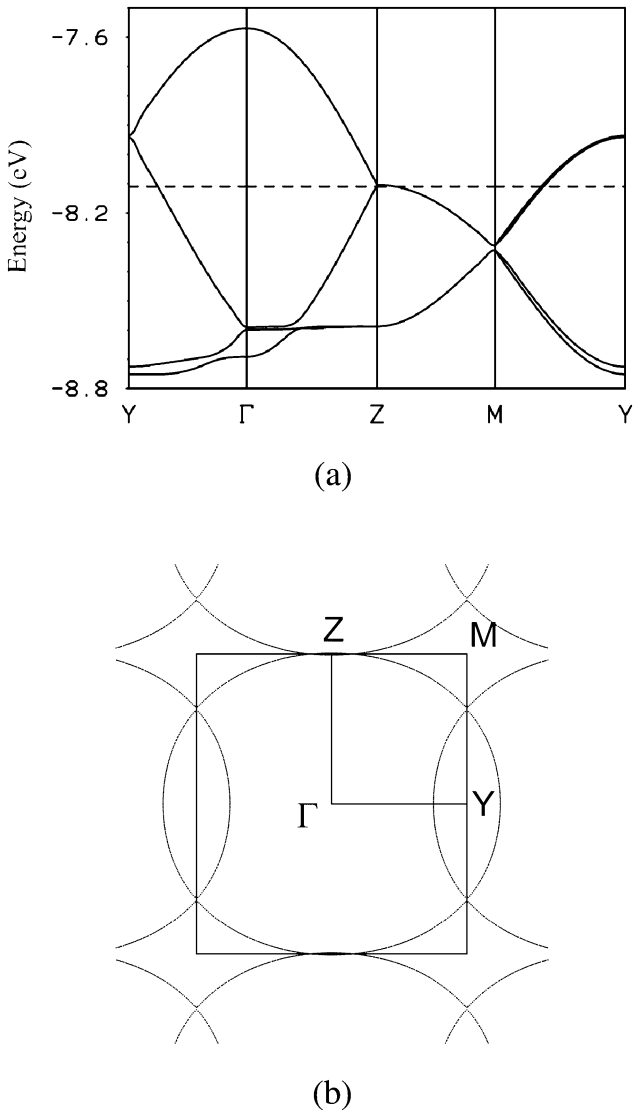

Fig. 4 Electronic structure of **1**: (a) Calculated band structure for a donor layer where the dashed line refers to the Fermi level; (b) calculated Fermi surface for a donor layer. $\boldsymbol{\Gamma} = (0, 0)$, $\boldsymbol{Y} = (b^*/2, 0)$, $\boldsymbol{Z} = (0, c^*/2)$ and $\boldsymbol{M} = (b^*/2, c^*/2)$.

Since there are four donors per repeat unit of the layer and the anion has a charge of −1, there must be two holes in the four HOMO-based bands of Fig. 4a. The symmetry of the lattice is such that the two upper bands must touch at ***Z***. Since the HOMO–HOMO interactions are strong (see Table 2), these bands are dispersive and partially filled. Thus, the salt must exhibit metallic behavior as experimentally found. The calculated Fermi surface is shown in Fig. 4b. It results from the superposition of almost circular pieces with an area of one cross-section of the Brillouin zone (BZ). This Fermi surface would be similar to that of the classical α-phases if the hybridization between circular portions was stronger: in that case the closed portions around the ***Y*** point would decrease its area and remain more 'isolated' from a slightly warped *pseudo* one-dimensional component parallel to the b^*-direction. In any case, the Fermi surface shown in Fig. 4b does not exhibit any flat portion which could be associated with a nesting vector, as is the case in the classical α-phases, so that this salt should be a very stable 2D metal. Thus, the conducting properties of **1** should be very different from those of the α-(BEDT-TTF)$_4$[MHg(SCN)$_4$] (M = NH_4^+, K^+, Rb^+ and Tl^+) family.

The comparison of the crystal and electronic structures of **1** and those of the α-(BEDT-TTF)$_4$[MHg(SCN)$_4$] (M = NH_4^+, K^+, Rb^+ and Tl^+) family clearly indicate that the origin of this difference is mainly related to the differences in the stacking mode. In **1** there is only one type of stack with practically identical donors (the HOMO energies of the two donor molecules are very close, −8.496 and −8.482 eV) and very uniform as well as quite strong interactions. In contrast, a strong dimerization occurs in the salts of the α-(BEDT-TTF)$_4$[MHg(SCN)$_4$] (M = NH_4^+, K^+, Rb^+ and Tl^+) family, where one interaction becomes very weak. An in-depth analysis of the electronics structure of these phases[28] clearly showed that this dimerization is responsible for the *pseudo*-one-dimensional behavior along the interstacks direction. In addition, in those salts the interstack interactions are less uniform than in **1**. Finally, in α-(BEDT-TTF)$_4$[MHg(SCN)$_4$] (M = NH_4^+, K^+, Rb^+ and Tl^+) there are three crystallographically nonequivalent donor molecules with different HOMO energies and in some cases this difference may be quite pronounced. These facts are responsible for the gap openings at the ***Y*** and ***Z*** points, which determine the quite different character of the Fermi surface of the two types of α salts and, ultimately, their different conducting properties.

Magnetotransport properties

The study of R *vs* T along the *a* axis showed that **1** is a molecular metal stable down to 0.4 K (Fig. 5). At room temperature out-of-plane resistivity of this sample $\rho_\perp$ (300K) is equal to about 80 Ω cm, which is typical of highly anisotropic quasi two-dimensional organic conductors. The magnetotransport properties of the single crystals were examined at $T = 0.4$ K. The $R(B)$ dependence is presented in Fig. 6a for the field orientation $B \| a$. Shubnikov-de Haas (SdH) oscillations, which are quite clear in the expanded scale insert, were found at $B > 10$ T. The oscillation spectrum consists of two main modes with considerably different frequencies. One can see these two oscillation modes

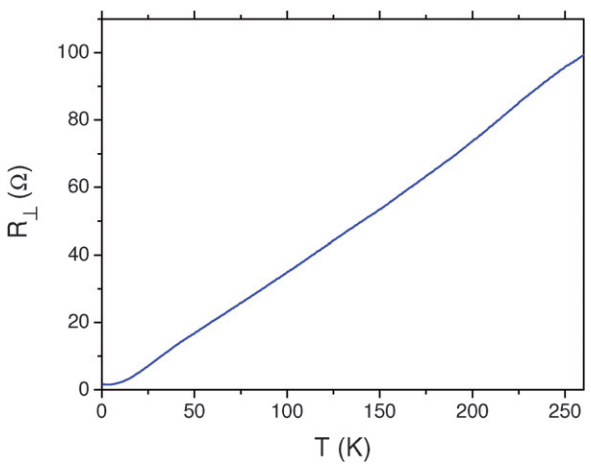

Fig. 5 Temperature dependence for the transverse ($R_\perp$) resistance of the single crystal **1**.

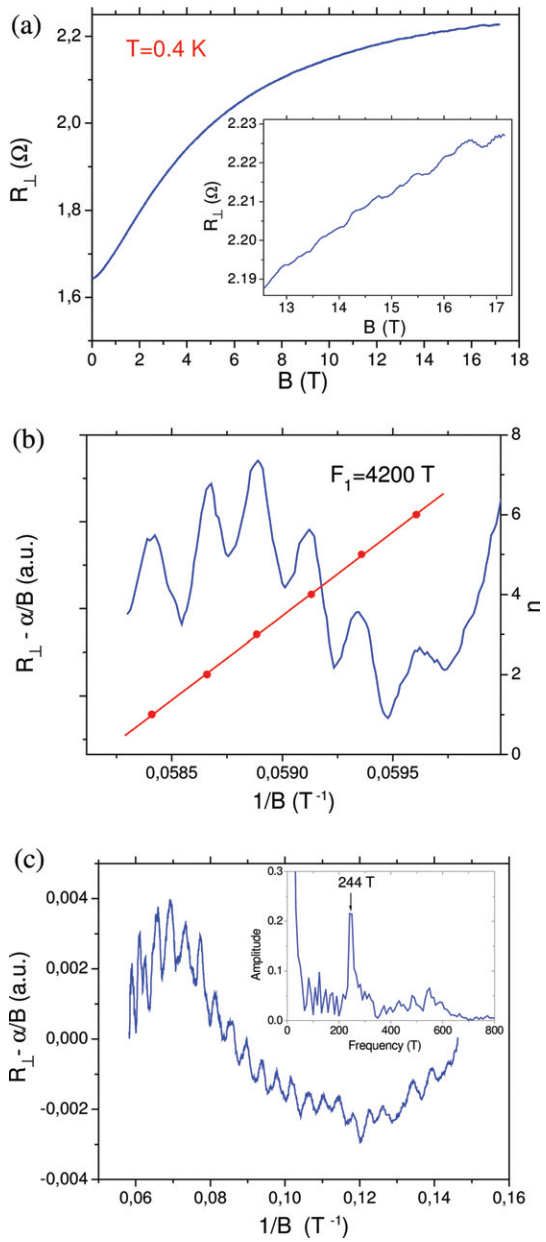

Fig. 6 (a) Magnetic field dependence for the transverse resistance of the single crystal **1** at $T = 0.4$ K. The insert makes clear the oscillatory behavior of the resistance at $B > 10$ T. (b) High frequency component ($F_1 = 4200$ T) of the Shubnikov-de-Haas oscillations at $B > 16$ T. The straight line corresponds to the oscillation maxima positions as a function of the number n and demonstrates the periodicity of the oscillations in $1/B$ scale. (c) Low frequency component of the Shubnikov-de-Haas oscillations. The Fourier spectrum with a fundamental frequency $F_2 = 244$ T is shown in the insert.

separately in Figs. 6b and c, where the resistance is plotted as a function of the reciprocal magnetic field. To see the oscillations more clearly, the monotonous component of the $R(1/B)$ dependence is subtracted from the curves for both figures. The high frequency component $F_1 = 4200$ T is observed in the field interval (16–17.2) T (Fig. 6b). The low frequency component $F_2 = 244$ T, observed in a more wide field region of (10–17.2) T, is shown in Fig. 6c.

According to our energy band calculations, SdH oscillations at $B\|a$ could result from two kinds of orbits in k-space: the classical orbit α determined by the lens around the Y point of the BZ, and the magnetic breakdown orbit β – ellipse around the point Γ of the BZ (see Fig. 4). The area of the latter orbit must be equal to 100% of the cross-section of the BZ whereas the area of the former one is about 11%. From these area values and from the measured lattice parameters one can calculate the fundamental frequencies of the SdH oscillations $F_\alpha = 482$ T and $F_\beta = 4090$ T, respectively. The larger experimentally observed frequency F_1 is in a fairly good agreement with the value F_β (the difference is about 2.5%), while the frequency of the long-period oscillations F_2 is about twice smaller than the value of F_α, *i.e.* the experimentally determined value for the lens area is about 6% of the cross-section of the BZ. The difference between the calculated and experimental values is a bit too large to be attributed solely to deficiencies in the computational scheme which generally leads to results in good agreement with experiment. The possible reason for the difference can be assumed. Whereas the Fermi surface has been calculated on the basis of the crystal structure at room temperature, the SdH measurements have been carried out at very low temperature. The area of the lens decreases when the hybridization of the large ellipses increases, something which occurs when the stacks are less uniform. Thus we believe that a likely possibility is that the stacks become somewhat less uniform as a result of thermal contraction. Low temperature X-ray work is needed in order to test this suggestion.

Analysis of the magnetic susceptibility and evaluation of exchange parameters

The temperature variation of the effective magnetic moment $\mu_{\text{eff}}(T)$ of **1** is shown in Fig. 7. We have simulated the magnetic susceptibility of **1** in terms of a conventional model assuming isotropic exchange interactions between Mn^{2+} ions. There is some difficulty in the analysis of the magnetic properties of **1** due to the fact that Mn^{2+} ions form infinite zigzag chains composed of corner-sharing triangles rather than simple linear chains (see Fig. 2a). In contrast with the situation for linear chains, not much is known about the magnetic behavior of triangular antiferromagnetic zigzag chains; to the best of our knowledge, no computational approaches are available in the literature for such chains. In view of this situation, we use finite fragments of the triangular chain to reproduce the experimental temperature dependence of the magnetic susceptibility and to evaluate the exchange parameters. Namely, calculations are performed for a cluster composed of five Mn^{2+} ions forming a double triangle, which represents the minimal translational unit of the zigzag chain (see Fig. 7a). In this cluster, the magnetic coupling between Mn^{2+} ions is described by the spin Hamiltonian

$$H_{\text{ex}} = -2J_1(S_1S_2 + S_2S_3 + S_3S_4 + S_4S_5) - 2J_2(S_1S_3 + S_3S_5) \quad (1)$$

involving two exchange parameters, J_1 and J_2 (Fig. 7a), where all spins S_n have the same value of 5/2 corresponding to the high-spin $^6A_1$ ground state of Mn^{2+} ions. The energy spectrum of spin levels of this cluster is obtained from the numerical diagonalization of the spin Hamiltonian (1) and then the magnetic susceptibility is calculated using the van Vleck equation. The best

fit to the experimental temperature dependence of the effective magnetic moment is obtained with the antiferromagnetic exchange parameters $J_1 = -1.35$ and $J_2 = -0.85$ cm^{-1}. It is important to note that at high temperatures ($T > 100$ K) a noticeable deviation is observed between calculated (μ_{calc}) and experimental (μ_{exp}) magnetic moment (Fig. 7 a, curve 2); in fact, at room temperature μ_{exp} is somewhat higher than the magnetic moment of isolated Mn^{2+} ion (6.03 μ_B and 5.92 μ_B, respectively). This may be due to the paramagnetic contribution of conduction electrons in the radical cation salt. Alternatively (and even more likely), this may be caused by a nonstoichiometry of polycrystalline samples of **1**, in which the ratio between organic radicals and manganese ions can deviate from the nominal value of 1 : 1. To examine the latter suggestion, we have performed calculations, in which the ratio β = Mn/BEDT-TTF is allowed to vary. A very good fit is obtained with $J_1 = -1.70$, $J_2 = -1.50$ cm^{-1}, and $\beta = 1.18$ (Fig. 7a, curve 3). The origin of non-stoichiometry of **1** can easily be explained by the presence of some fraction of other phases with $\beta > 1$ in the polycrystalline samples. The majority of the studied crystals revealed a metallic type conductivity characteristic of **1**. However, a temperature dependence of semiconducting type was observed on one of the measured crystals. The latter was not identified by an X-ray analysis because it had low quality.

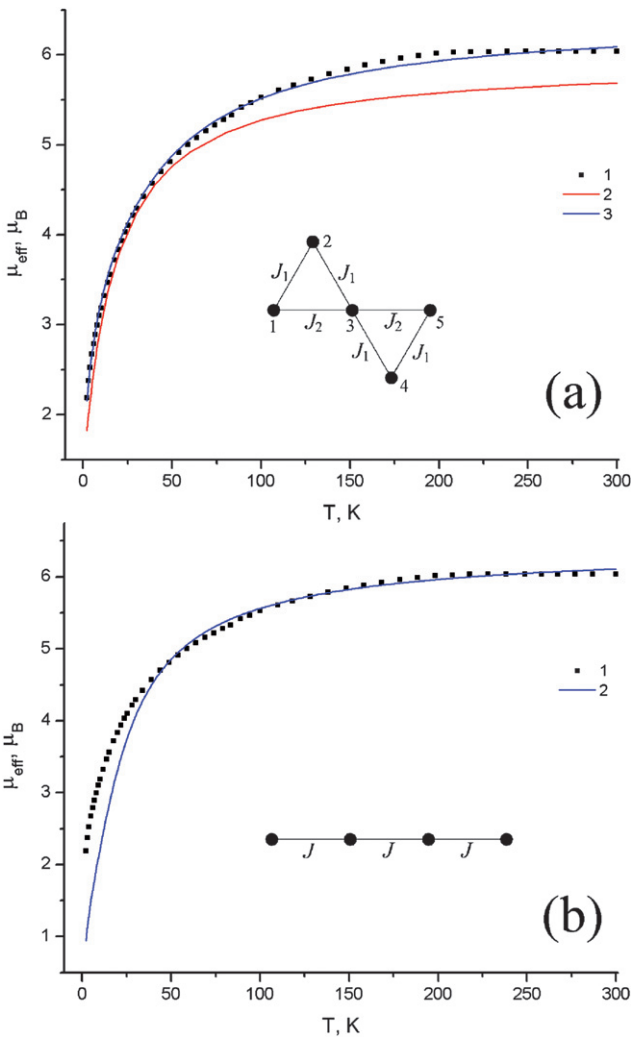

Fig. 7 Experimental and calculated temperature variation of the effective magnetic moment $\mu_{eff}(T)$ of **1**: (a) results obtained for a double triangle cluster, (1) experimental, (2) calculated with $J_1 = -1.35$, $J_2 = -0.85$ cm^{-1} and $\beta = 1$, (3) calculated with $J_1 = -1.70$, $J_2 = -1.50$ cm^{-1}, and $\beta = 1.18$; (b) results obtained for a linear antiferromagnetic chain, (1) experimental and (2) calculated with $J = -6.90$ cm^{-1} and $\beta = 1.18$ (see the text for details).

In addition, we have simulated the $\mu_{eff}(T)$ curve using an analytical approximation for the magnetic susceptibility of a linear antiferromagnetic chain with a unique exchange parameter J, (Fig. 7b).[30] In this case, the best fit corresponds to $J = -6.90$ cm^{-1} and $\beta = 1.18$ (Fig. 7b, curve 2).

To verify the consistency of the fitting procedure, we have estimated J_1 and J_2 using a microscopic many-electron superexchange model described by Mironov *et al.*[31] In these calculations, we used an Mn → Mn charge-transfer energy $U = 10$ eV and the Racah parameters $B = 700$ and $C = 3000$ cm^{-1}. The set of electron transfer parameters for magnetic 3d orbitals of Mn is obtained from extended Hückel calculations[19] using the projection procedure described by Lee.[32] The calculated exchange parameters $J_1 = -4.3$ and $J_2 = -3.9$ cm^{-1} are in reasonable agreement with the fitted parameters (Fig. 7a). The absolute values of the calculated exchange parameters are approximately twice as large as the values of the exchange parameters obtained from the double triangle model (Fig. 7a) with a very similar J_1/J_2 ratio; on the other hand, the calculated J_1 and J_2 parameters are smaller than J obtained from the linear chain model (Fig. 7b). We can therefore conclude that the calculated and fitted exchange parameters fall into the same energy range and have the same sign (antiferromagnetic). Small antiferromagnetic exchange parameters are generally consistent with the behavior of the $\mu_{eff}(T)$ curve, which is typical of an overall weak antiferromagnetic coupling between high-spin magnetic centers.

Conclusion

The molecular metal α-(BEDT-TTF)$_2$[$Mn_2Cl_5(H_2O)_5$], which contains conducting organic layers and polymeric $[Mn_2Cl_5(H_2O)_5]^-_\infty$ chains responsible for the magnetic properties, is an interesting new member of the family of BEDT-TTF-based radical cation salts with chloromanganate(II) anions. It is an α-phase very different from the classical ones of the α-(BEDT-TTF)$_4$[$MHg(SCN)_4$] (M = NH_4^+, K^+, Rb^+ and Tl^+) family because the topology of radical cation stacks leads to a set of very isotropic HOMO–HOMO intermolecular interactions. Consequently, this salt is a stable 2D metal. The 2D character of the conductivity is confirmed by measurements of Shubnikov-de Haas oscillations at 0.4 K in magnetic fields above 10 T. The metallic behavior of the paramagnetic conducting BEDT-TTF sub-system and antiferromagnetic correlations in the polymeric anion layers are found to coexist for a wide temperature range but the interference among them is not clear yet. The crystal structure of **1** suggests a significant interaction of the conducting and magnetic layers due to the presence of rather strong hydrogen bonds coupling them. However, our results indicate that the experimental magnetic susceptibility is quantitatively reproduced in terms of an isolated Mn chain approach which implies that there is no coupling between the localized $S = 5/2$

spins of the Mn^{2+} ions and the conducting electrons of the BEDT-TTF layers.

Acknowledgements

This work was partially supported by the RFBR-JSPS grant 07-03-91207, the RFBR grants 09-02-00241 and 09-02-00852, the Program of Russian Academy of Sciences, the Spanish Ministerio de Educación y Ciencia (Project FIS2006-12117-C04-01) and the Generalitat de Catalunya (2005 SGR 683). We thank L. I. Buravov for the preliminary conductivity measurements and R. B. Morgunov for the SQUID measurements and for discussions.

References

1 (*a*) T. Ishiguro, R. Yamaji and G. Saito. *Organic superconductors*, Springer-Verlag, Berlin, 1988; (*b*) E. Coronado and P. Day, *Chem. Rev.*, 2004, **104**, 5419; (*c*) T. Enoki and A. Miyazaki, *Chem. Rev.*, 2004, **104**, 5449; (*d*) H. Kobayashi, H. Cui and A. Kobayashi, *Chem. Rev.*, 2004, **104**, 5265; (*e*) L. Ouahab, *Organic Conductors, Superconductors and Magnets: From Synthesis to Molecular Electronics*, ed. L. Ouahab and E. Yagubskii. Kluwer Academic PublishersDordrecht/Boston/London. 2003. P. 99; (*f*) G. Saito and Y. Yoshida, *Bull. Chem. Soc. Jpn.*, 80, p. 1.

2 (*a*) M. Kurmoo, T. Mallah, P. Day, I. Marsden, M. Allan, R. H. Friend, F. L. Pratt, W. Hayers, D. Chasseau, J. Gaultier and G. Bravic, *The Physics and Chemistry of Organic Superconductors*, ed. G. Saito and S. Kagoshima. *Springer Proc. Phys. V. 51*. Springer-VerlagBerlin Heidelberg. 1990. P. 290; (*b*) A. V. Gudenko, V. B. Ginodman, V. E. Korotkov, A. V. Koshelap, N. D. Kushch, V. N. Laukhin, L. P. Rozenberg, A. G. Khomenko, R. P. Shibaeva and E. B. Yagubskii, *The Physics and Chemistry of Organic Superconductors*, ed. G. Saito and S. Kagoshima. *Springer Proc. Phys. V. 51*. Springer-VerlagBerlin Heidelberg. 1990. P. 364; (*c*) P. Day, M. Kurmoo, T. Mallah, R. H. Friend, F. L. Pratt, W. Hayers, D. Chasseau, J. Gaultier, G. Bravic and L. Ducasse, *J. Am. Chem. Soc.*, 1992, **114**, 10722.

3 K. Kikuchi, H. Nishikawa, I. Ikemoto, T. Toita, H. Akutsu, S. Nakatsuji and Y. Yamada, *J. Solid State Chem.*, 2002, **168**, 503.

4 E. Coronado, L. R. Falvello, J. R. Galán-Mascarós, C. Giménez-Saiz, C. J. Gómez-García, V. N. Laukhin, A. Pérez-Benítez, C. Rovira and J. Veciana, *Adv. Mater.*, 1997, **9**, 984.

5 (*a*) A. Dubrovskii, T. Prokhorova, N. Spitsina, A. Kazakova, N. Kushch, L. Buravov, S. Simonov, L. Zorina, S. Khasanov, R. Morgunov, O. Drozdova, Y. Tanimoto, R. Shibaeva and E. Yagubskii, *J. Low Temp. Phys.*, 2006, **142**, 137; (*b*) R. P. Shibaeva, S. S. Khasanov, L. V. Zorina and S. V. Simonov, *Crystallography Reports*, 2006, **51**, 949.

6 T. G. Prokhorova, S. V. Simonov, S. S. Khasanov, L. V. Zorina, L. I. Buravov, R. P. Shibaeva, E. B. Yagubskii, R. B. Morgunov, D. Fortynowicz and R. Swietlik, *Synth. Met.*, 2008, **158**, 749.

7 H. Yamochi, T. Kawasaki, Y. Nagata, M. Maesato and G. Saito, *Mol. Cryst. Liq. Cryst.*, 2002, **376**, 113.

8 E. Coronado, J. R. Galán-Mascarós, C. Giménez-Saiz, C. J. Gómez-García, E. Martinez-Ferrero, M. Almeida and E. B. Lopes, *Adv. Mater.*, 2004, **16**, 324.

9 (*a*) M. Kurmoo, A. W. Graham, P. Day, S. J. Coles, M. B. Hursthouse, J. L. Caulfield, J. Singleton, F. L. Pratt, W. Hayes, L. Ducasse and P. Guionneau, *J. Am. Chem. Soc.*, 1995, **117**, 12209; (*b*) S. Rashid, S. S. Turner, P. Day, J. A. K. Howard, P. Guionneau, E. J. L. McInnes, F. E. Mabbs, R. J. H. Clark, S. Firth and T. J. Biggs, *J. Mater. Chem.*, 2001, **11**, 2095; (*c*) A. Audouard, V. N. Laukhin, L. Brossard, T. G. Prokhorova, E. B. Yagubskii and E. Canadell, *Phys. Rev. B*, 2004, **69**, 144523; (*d*) E. Coronado, S. Curreli, C. Giménez-Saiz and C. J. Gómez-García, *J. Mater. Chem.*, 2005, **15**, 1429.

10 H. Fujiwara, H. Kobayashi, E. Fujiwara and A. Kobayashi, *J. Am. Chem. Soc.*, 2002, **124**, 6816.

11 N. D. Kushch, E. B. Yagubskii, M. V. Kartsovnik, L. I. Buravov, A. D. Dubrovskii, A. N. Chekhlov and W. Biberacher, *J. Am. Chem. Soc.*, 2008, **130**, 7238.

12 E. S. Choi, D. Graf, J. S. Brooks, J. Yamada, H. Akutsu, K. Kikuchi and M. Tokumoto, *Phys. Rev. B*, 2004, **70**, 024517.

13 (*a*) S. Uji, H. Shinagawa, T. Terashima, T. Yakabe, Y. Terai, M. Tokumoto, A. Kobayashi, H. Tanaka and H. Kobayashi, *Nature*, 2001, **410**, 908; (*b*) L. Balikas, J. S. Brooks, K. Storr, S. Uji, M. Tokumoto, H. Tanaka, H. Kobayashi, A. Kobayashi, V. Barzykin and L. P. Gorkov, *Phys. Rev. Lett.*, 2001, **87**, 067002.

14 (*a*) E. Coronado, J. R. Galán-Mascarós, C. J. Gómez-García and V. Laukhin, *Nature*, 2000, **408**, 447; (*b*) A. Alberola, E. Coronado, J. R. Galán-Mascarós, C. Giménez-Saiz and C. J. Gómez-García, *J. Am. Chem. Soc.*, 2003, **125**, 10774.

15 (*a*) T. Mori and H. Inokuchi, *Bull. Chem. Soc. Jpn.*, 1988, **61**, 591; (*b*) T. Naito, T. Inabe, K. Takeda, K. Awaga, T. Akutagawa, T. Hasegawa, T. Nakamura, T. Kakiuchi, H. Sawa, T. Yamamoto and H. Tajima, *J. Mater. Chem.*, 2001, **11**, 2221; (*c*) H. Miyasaka, Y. Yoshino, T. Ishii, R. Kanehama, T. Manabe, M. Yamashita, H. Nishikawa and I. Ikemoto, *J. Solid State Chem.*, 2002, **168**, 418; (*d*) T. Naito and T. Inabe, *J. Solid State Chem.*, 2003, **176**, 243; (*e*) W. Xu, R. Shen, C. M. Liu, D. Zhang and D. Zhu, *Synth. Met.*, 2003, **133–134**, 349; (*f*) T. Naito and T. Inabe, *Bull. Chem. Soc. Jpn.*, 2004, **77**, 1987.

16 Oxford Diffraction (2007), Oxford Diffraction Ltd., *Xcalibur CCD system, CrysAlisPro Software system, Version 1.171.32*.

17 G. M. Sheldrick, *Acta Crystallogr., Sect. A*, 2008, **64**, 112.

18 S. Khasanov, T. Prokhorova, S. Simonov, L. Zorina, L. Buravov, V. Zverev, R. Shibaeva and E. Yagubskii, *The 21st IUCr Sattelite Meeting "Molecular Crystals Exhibiting Exotic Functions"*, Osaka, Japan, August 21–22, 2008, p. P12.

19 M.-H. Whangbo and R. Hoffmann, *J. Am. Chem. Soc.*, 1978, **100**, 6093.

20 J. Ammeter, H.-B. Bürgi, J. Thibeault and R. Hoffmann, *J. Am. Chem. Soc.*, 1978, **100**, 3686.

21 A. Pénicaud, K. Boubekeur, P. Batail, E. Canadell, P. Auban-Senzier and D. Jérome, *J. Am. Chem. Soc.*, 1993, **115**, 4101.

22 P. L'Haridon and M. T. Le Bihan, *Acta. Crystallogr.*, 1973, **B29**, 2195.

23 (*a*) B. Morosin and E. J. Graebner, *Acta Crystallogr.*, 1967, **23**, 766; (*b*) R. Dingle, M. E. Lines and S. L. Holt, *Phys. Rev.*, 1969, **187**, 643.

24 S. J. Jensen, *Acta Chem. Scand.*, 1967, **21**, 889.

25 P. Guionneau, C. J. Kepert, G. Bravic, D. Chasseau, M. R. Truter, M. Kurmoo and P. Day, *Synth. Met.*, 1997, **86**, 1973.

26 M. V. Kartsovnik and V. N. Laukhin, *J. Phys. I*, 1996, **6**, 1753.

27 M. V. Kartsovnik, *Chem. Rev.*, 2004, **104**, 5737.

28 R. Rousseau, M.-L. Doublet, E. Canadell, R. P. Shibaeva, S. S. Khasanov, L. P. Rozenberg, N. D. Kushch and E. B. Yagubskii, *J. Phys. I*, 1996, **6**, 1527.

29 M.-H. Whangbo, J. M. Williams, P. C. W. Leung, M. A. Beno, T. J. Emge and H. H. Wang, *Inorg. Chem.*, 1985, **24**, 3500.

30 (*a*) J. W. Hall, Ph. D. Dissertation, Univ. North Carolina, Chapel Hill, NC 27514 (1977); (*b*) D. Bertran, E. Escriva and M. Drillon, *J. Chem Soc., Faraday Trans.*, 1982, **78**, 1773.

31 V. S. Mironov, L. F. Chibotaru and A. Ceulemans, *Phys. Rev. B*, 2003, **67**, 014424.

32 S. Lee, *J. Am. Chem. Soc.*, 1989, **111**, 7754.